Supplementary Information

Porous Cu/C Nanofibers Promote Electrochemical CO_2-to-Ethylene Conversion *via* High CO_2 Availability

Daewon Bae[1], Taemin Lee[1], Woosuck Kwon[1], Sang-Ho Oh[2] and Dae-Hyun Nam[1,*]

[1]Department of Energy Science and Engineering, Daegu Gyeongbuk Institute of Science and Technology (DGIST), Daegu 42988, Republic of Korea

[2]Department of Materials Science and Engineering, Seoul National University, Seoul 08826, Republic of Korea

*Corresponding author:

Dae-Hyun Nam

Department of Energy Science and Engineering

Daegu Gyeongbuk Institute of Science and Technology (DGIST)

E-mail: dhnam@dgist.ac.kr.

Electrospinning of Cu Precursor + Blended Polymer Nanofibers

The fabrication processes of all nanofibers required metal precursor solution and polymer solution for electrospinning. For the fabrication of Cu/CNFs (0%)_SO, Cu/CNFs (0%)_FR, 1.0 g of polyacrylonitrile (PAN) (Sigma-Aldrich, Mw: 150,000) was dissolved in 5 g of N, N-dimethyl formamide (DMF) (Sigma-Aldrich) for polymer solution. 1.0 g of copper acetate monohydrate (Sigma-Aldrich) was dissolved in 5 g of DMF for metal precursor solution. All solutions were heated to 120 ℃ and stirred overnight. Two solutions were mixed and stirred overnight at room temperature after the dissolution of the polymer and metal precursor. 0.6 g of PAN and 0.4 g of poly (methyl methacrylate) (PMMA) (Thermo Scientific) were blended in 5 g of DMF for fabricating Cu/CNFs (40%)_SO, Cu/CNFs (40%)_FR. 0.4 g of PAN and 0.6 g of PMMA were blended in 5 g of DMF for fabricating Cu/CNFs (60%)_SO, Cu/CNFs (60%)_FR. The metal precursor solutions were the same as those of fabricating Cu/CNFs (0%)_SO and Cu/CNFs (0%)_FR. The diameter-controlled Cu/CNFs (0%) were fabricated with 0.6g of PAN in 5 g of DMF solution and 0.6 g of copper acetate monohydrate in 5 g of DMF solution. All the heating and stirring steps after blending polymers were identical regardless of nanofibers. The mixed solutions were loaded into the syringe with a 21G metal needle tip. The syringe was pressed 1 mL/minute while the 17 kV of the voltage was applied to metal tips. The nanofibers were collected on a collector placed 15 cm away from the metal tip. All the chemical compounds were used without additional refinements.

Calcination of Electrospun Nanofibers

As-spun nanofibers were calcined at 700℃ for 4 hours with a ramping rate of 4℃ per minute under the oxygen (O_2) or argon (Ar) partial pressure-controlled atmosphere in thermal chemical vapor deposition (CVD) (Scientific Engineering). The gas partial pressure control was

performed after obtaining a high vacuum condition with a rotary pump (~10^{-2} torr) and turbo molecular pump (~10^{-6} torr). O_2 gas or Ar gas filled the chamber in CVD by mass flow controller (MFC) at a rate of 5 sccm and 10 sccm respectively. After getting 0.5 torr pressure, the gas flow was stopped by the MFC.

Material Characterization

The thermogravimetric curves were obtained from a thermogravimetric analyzer (TGA) (Discovery TGA 5500) with a ramping rate of 10°C per minute under a nitrogen gas atmosphere. The specific surface area, CO_2 adsorption ability, and pore size distributions of Cu/CNFs were examined by BELSORP-miniX. The data were calculated by the Brunauer-Emmett-Teller (BET) theory and the Barrett-Joyner-Halenda (BJH) model. The morphologies of the catalysts were confirmed by scanning electron microscope (SEM) (Hitachi, S-4800) and transmission electron microscope (TEM) with high-angle annular dark field imaging-scanning transmission electron microscopy-energy dispersive X-ray spectroscopy (HAADF-STEM-EDS) (FEI, Titan G2 ChemiSTEM Cs Probe). Carbon (C) shells on Cu particles were analyzed by FEI Titan TEM (THEMIS Z, Thermo Fisher Scientific) operated at 300 kV. The crystalline phase of Cu was found out by X-ray diffractometer (XRD) (Rigaku, Miniflex 600). The chemical properties of Cu/CNFs were analyzed by Raman spectroscopy (Renishaw, inVia Qontor) with 532 nm laser for analysis of C crystallinity and X-ray photoelectron spectroscope (XPS) (photoelectron spectrometer (XPS, Thermo Scientific Nexsa) for analysis of oxidation states of Cu surfaces. Hydrophobicity analyses of Cu/CNFs were conducted by contact angle measurement system (M.braun, DSA 100). Samples for analyzing hydrophobicity were prepared the following method. 10 mg of Cu/CNFs were dispersed with 2 mL of 2-propanol (IPA) (Sigma-Aldrich) and 5.12 μL of Aquivion ionomer (Sigma-Aldrich, EW 790, 25 wt %). The solution was coated

on a 4*4cm^2 size silicon wafer with an Ar-flowing air-brush gun. The hydrophobicity of Cu/CNFs was measured 3 times and averaged each data after measuring the bare silicon wafer.

The adsorbed *CO on electrodes during the CO_2RR were investigated by *in situ* Raman spectroscopy (XploRA^{TM} PLUS Raman spectrometer, HORIBA). The modified flow cell making for catalyst to contact with the laser was utilized with a water immersion objective lens (60×) and 785 nm laser. The laser was emitted for 10 seconds at each time and the analysis data were acquired ten times for all measurements.

Preparing Electrodes for CO_2RR and Measuring CO_2RR Performances

All the reactions were performed in 1 M KOH with Ag/AgCl reference electrode. Nickel foam was used to a counter electrode. Anion exchange membrane (Fuelcell, Fumasep FAA-3-PK-75) was used due to alkaline electrolyte. The potential applied with Ag/AgCl electrode was converted to that with a reversible hydrogen electrode (RHE). The conversion was calculated by the following equation.

$$E_{RHE} = E_{Ag/AgCl} + 0.1976\ (E^0) + 0.059 \times pH + i \times R_S \times 0.8$$

R_S is a resistance of solution and was obtained by electrochemical impedance spectroscopy (EIS) with a potentiostat (Autolab, PGSTAT204). The catalytic performances were analyzed by chrono amperometry with the potentiostat. Gas and liquid products were analyzed by gas chromatography (GC) (INFICON, Micro GC Fusion) with two separated thermal conductivity detectors (TCDs) and nuclear magnetic resonance spectroscopy (NMR) (Bruker, AVANCE III 400). Quantity analyses of gas products were calculated with external standards. Dimethyl sulfoxide was taken as an internal standard for quantity analyses of each liquid product. The operation time was all an hour. All gas products from each sample were

analyzed three times at 5 min, 30 min, and 55 min. They were averaged. The Faradaic efficiency (FE) for each product was calculated in the following equation.

$$\text{Faradaic efficiency (\%)} = \frac{z*n*F}{Q}$$

z and n are the number of transferred electrons and moles of products. n is calculated by multiplying product concentration and gas flow rate for gas products, and by multiplying product concentration and volume of electrolyte for liquid products. F is the Faradaic constant and Q is the input charge. The standard deviations of every product displayed by the error bar were from three independent samples. The CO_2 ratio was controlled by modifying flow rate of CO_2 and Ar respectively *via* MFC.

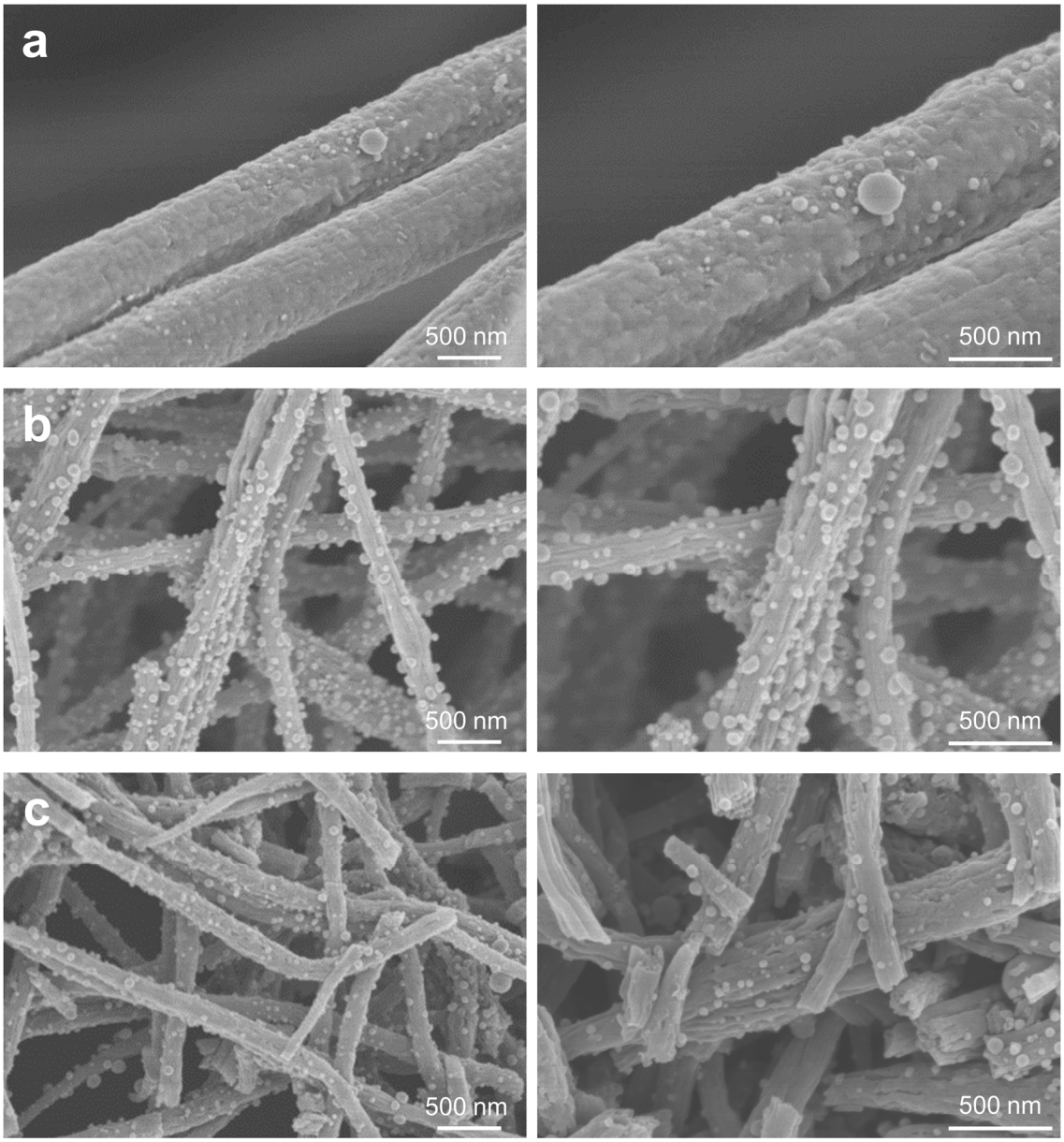

Fig. S1 Low magnified SEM images of Cu/CNFs (*X*%)_FR. (a) Cu/CNFs (0%)_FR, (b) Cu/CNFs (40%)_FR, and (c) Cu/CNFs (60%)_FR.

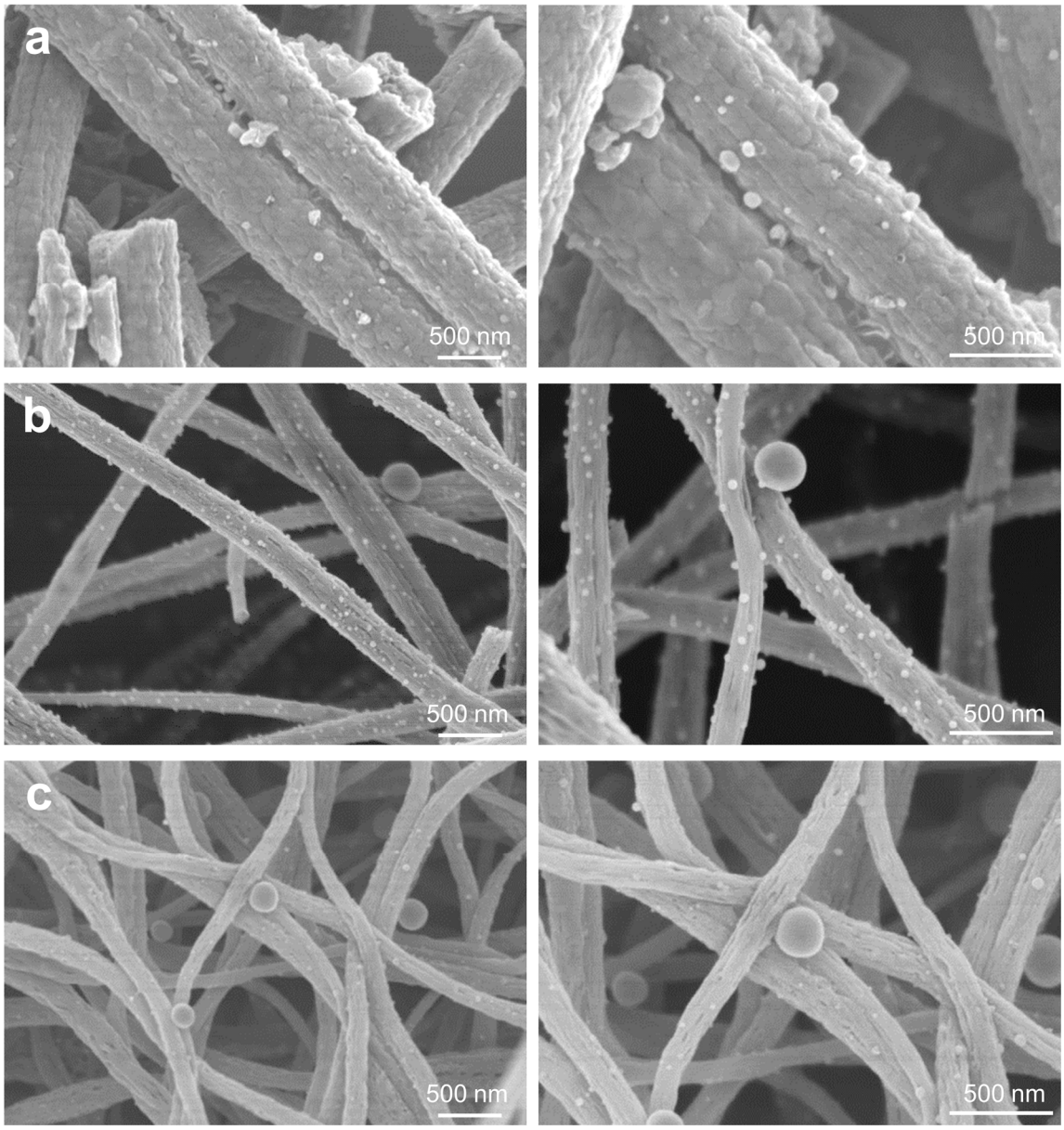

Fig. S2 Low magnified SEM images of Cu/CNFs (*X*%)_SO. (a) Cu/CNFs (0%)_SO, (b) Cu/CNFs (40%)_SO, and (c) Cu/CNFs (60%)_SO.

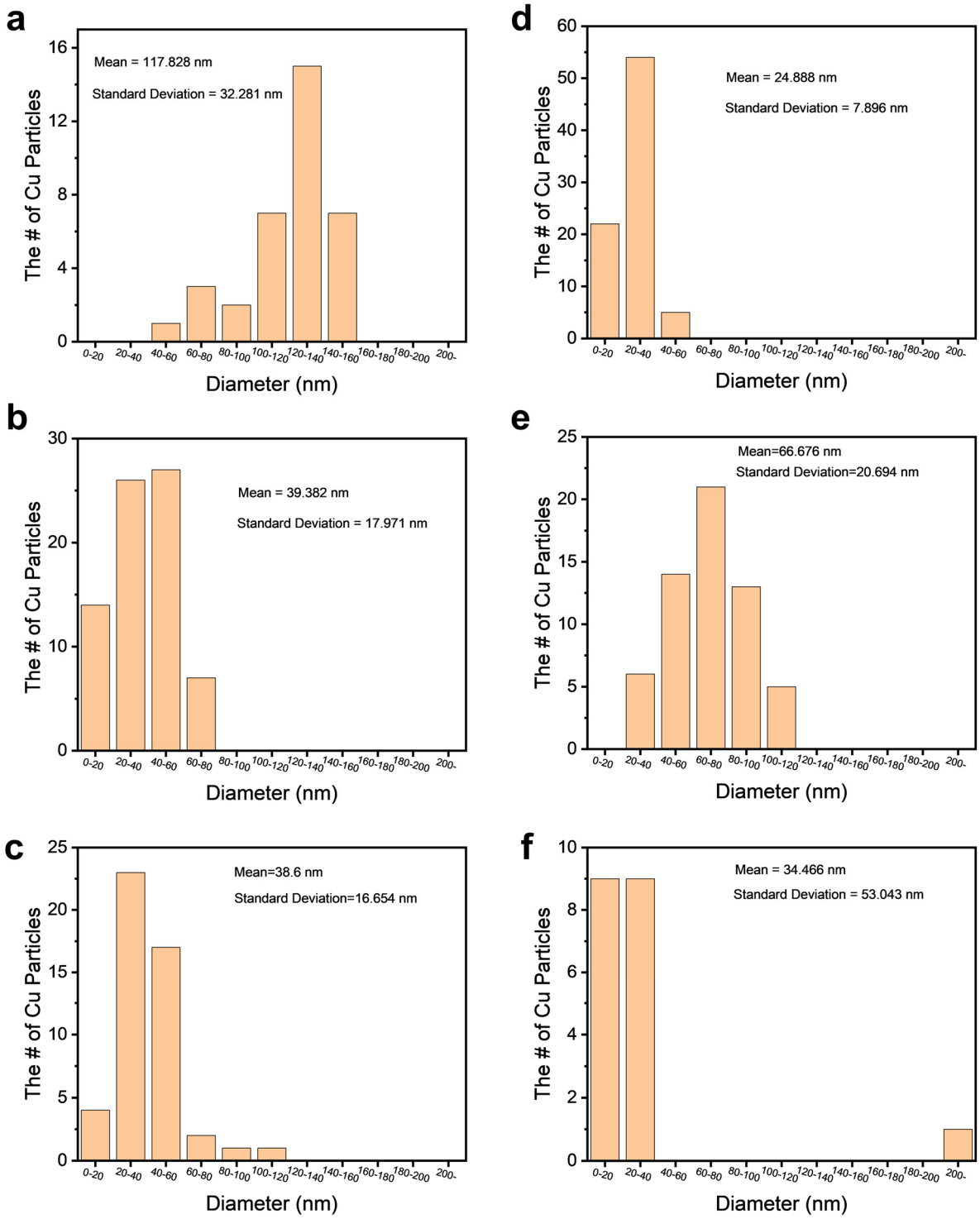

Fig. S3 Cu particle sizes distributions in Cu/CNFs represented by histograms. (a) Cu/CNFs (0%)_FR, (b) Cu/CNFs (40%)_FR, (c) Cu/CNFs (60%)_FR, (d) Cu/CNFs (0%)_SO, (e) Cu/CNFs (40%)_SO, and (f) Cu/CNFs (60%)_SO. Cu particle sizes were analyzed based on TEM images.

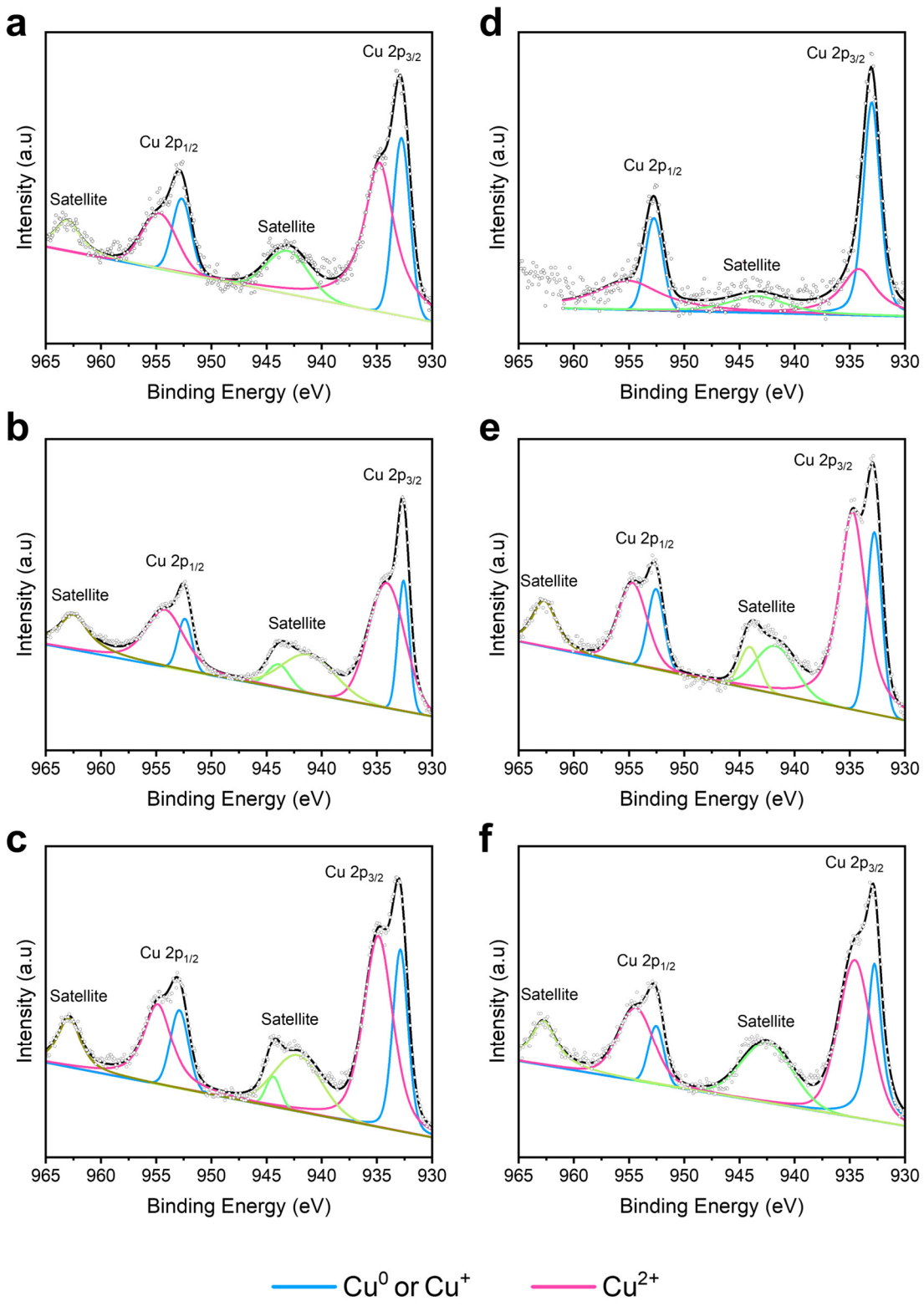

Fig. S4 XPS about Cu 2p for analyzing Cu oxidation states of (a) Cu/CNFs (0%)_FR, (b) Cu/CNFs (40%)_FR, (c) Cu/CNFs (60%)_FR, (d) Cu/CNFs (0%)_SO, (e) Cu/CNFs (40%)_SO, (f) Cu/CNFs (60%)_SO. The Cu $2p_{3/2}$ peaks were deconvoluted as Cu^0 or Cu^+ (~932.4 eV) and Cu^{2+} (~934.5 eV). The Cu $2p_{1/2}$ peaks were deconvoluted as Cu^0 or Cu^+ (~952.5 eV) and Cu^{2+} (~955 eV).[1, 2]

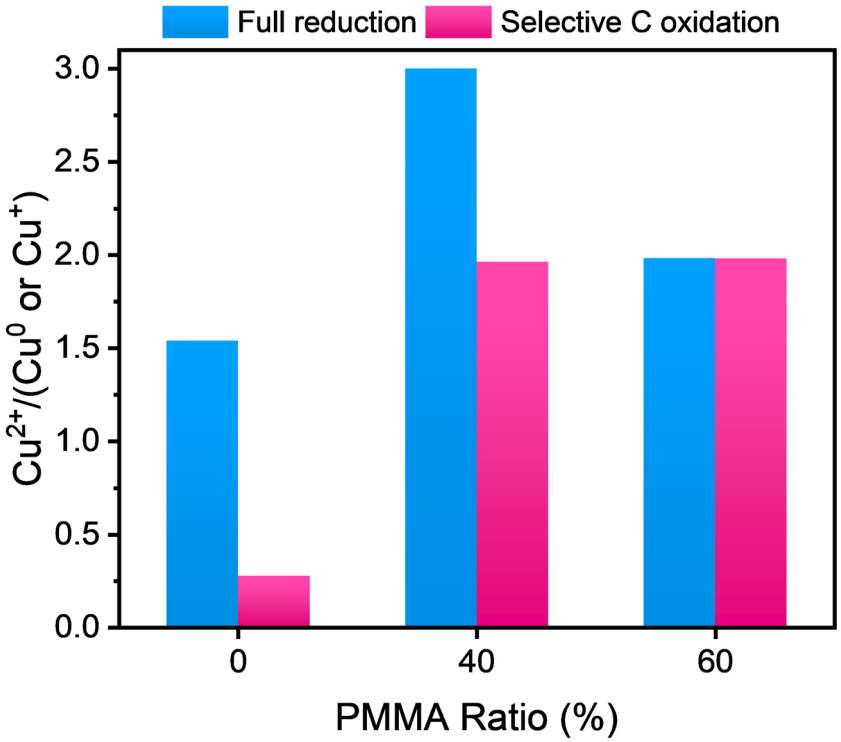

Fig. S5 Integral area ratio between 'Cu^{2+}' and 'Cu^0 or Cu^+' (Cu^{2+}/ (Cu^0 or Cu^+)) about Cu particles analyzed by XPS about Cu 2p in fabricated Cu/CNFs. The area was calculated from Cu $2p_{3/2}$.

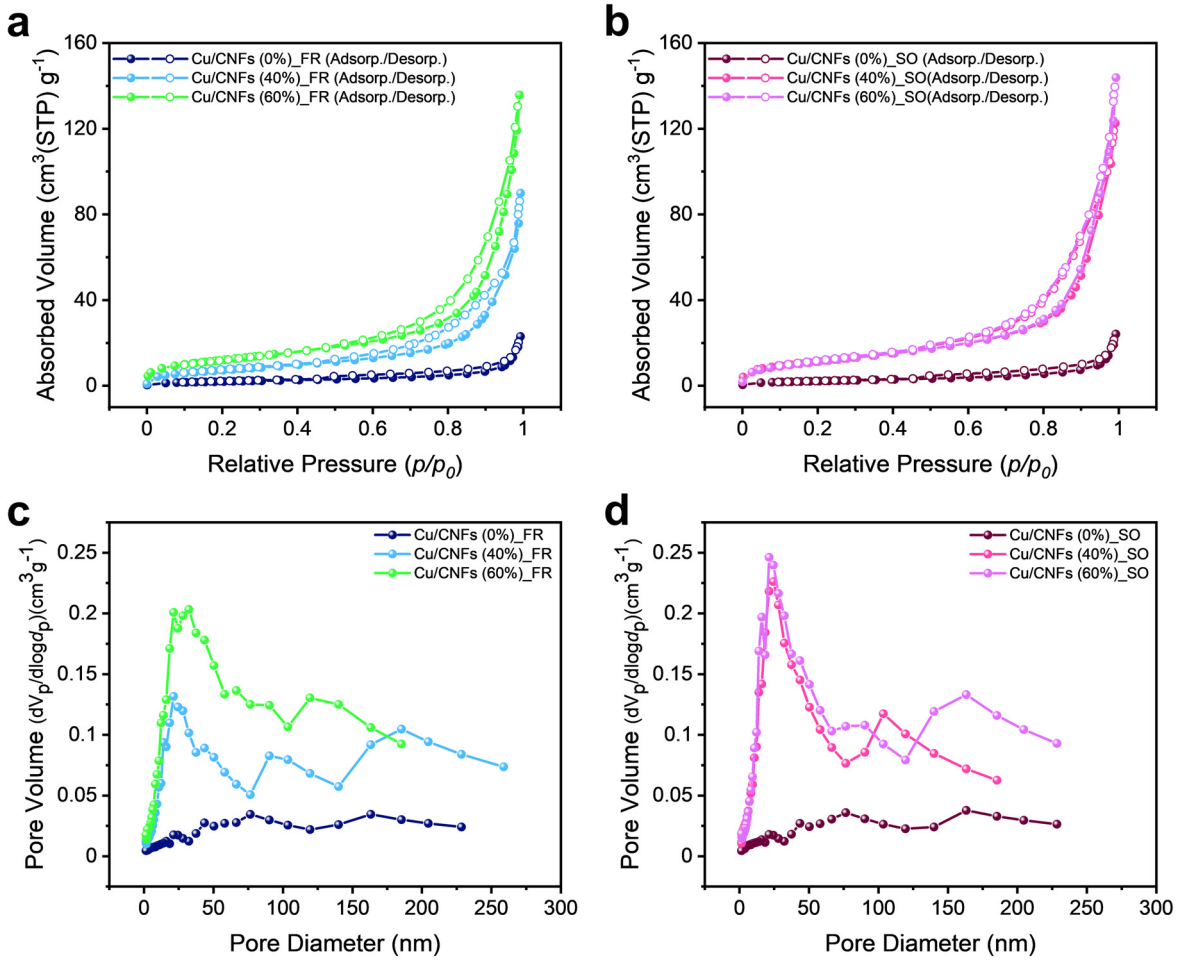

Fig. S6 N_2 adsorption and desorption graphs of (a) Cu/CNFs (*X*%)_FR and (b) Cu/CNFs (*X*%)_SO. BJH plots of (c) Cu/CNFs (*X*%)_FR and (d) Cu/CNFs (*X*%)_SO.

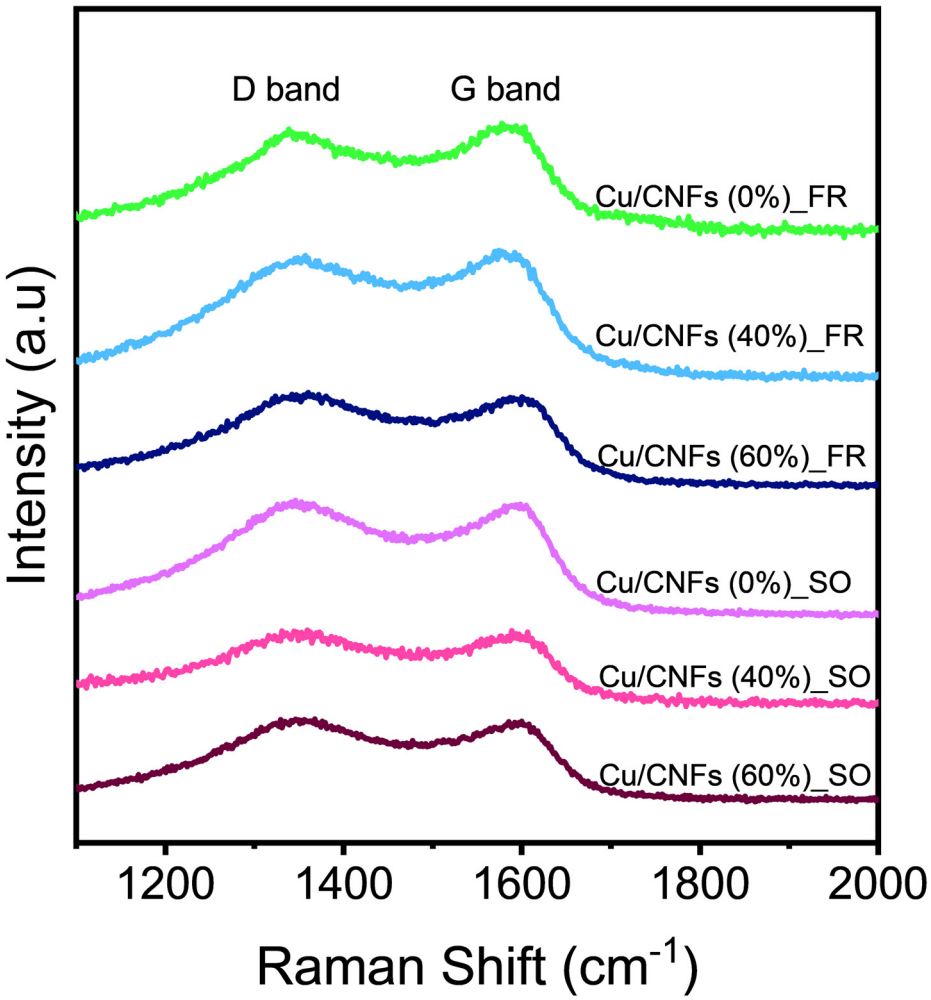

Fig. S7 Raman spectra of Cu/CNFs in the range from 1100-2000 cm^{-1} for analyzing C crystallinity. Calcination conditions affected PAN conversion to crystalline C.

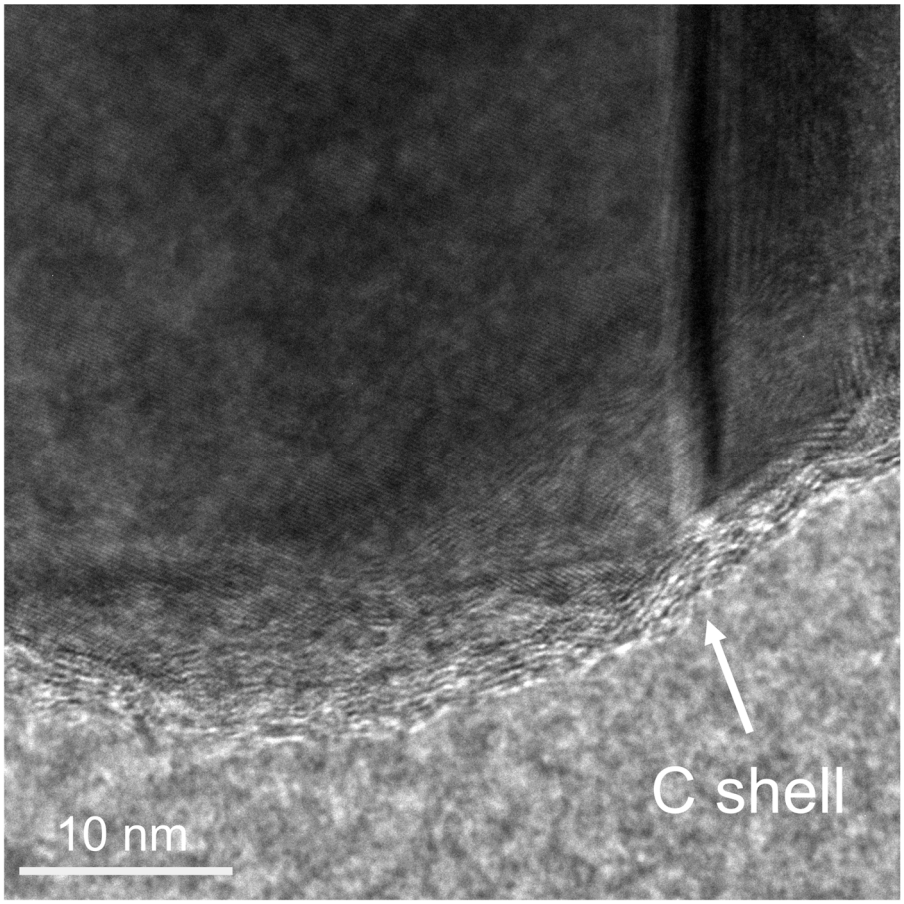

Fig. S8 TEM image of C shell on Cu nanoparticle in Cu/CNFs (0%)_SO. The thickness of C shell is about 2 nm.

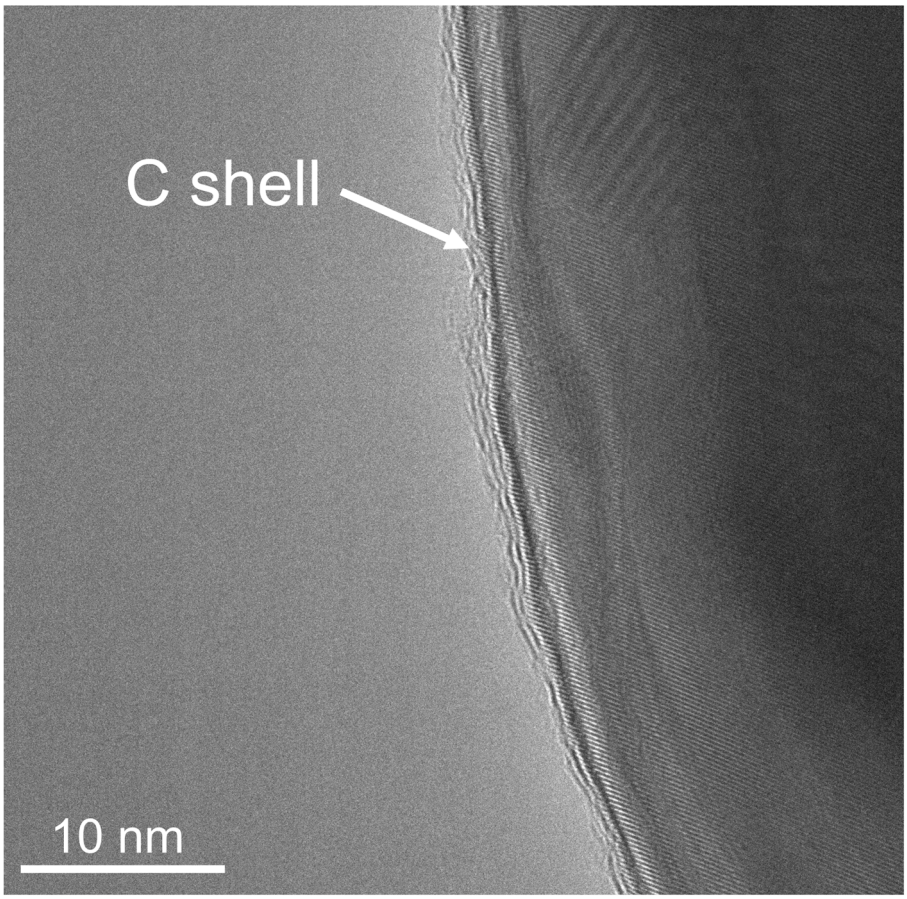

Fig. S9 HRTEM image of C shell on Cu nanoparticle in Cu/CNFs (40%)_SO. The thickness of C shell is about 1 nm.

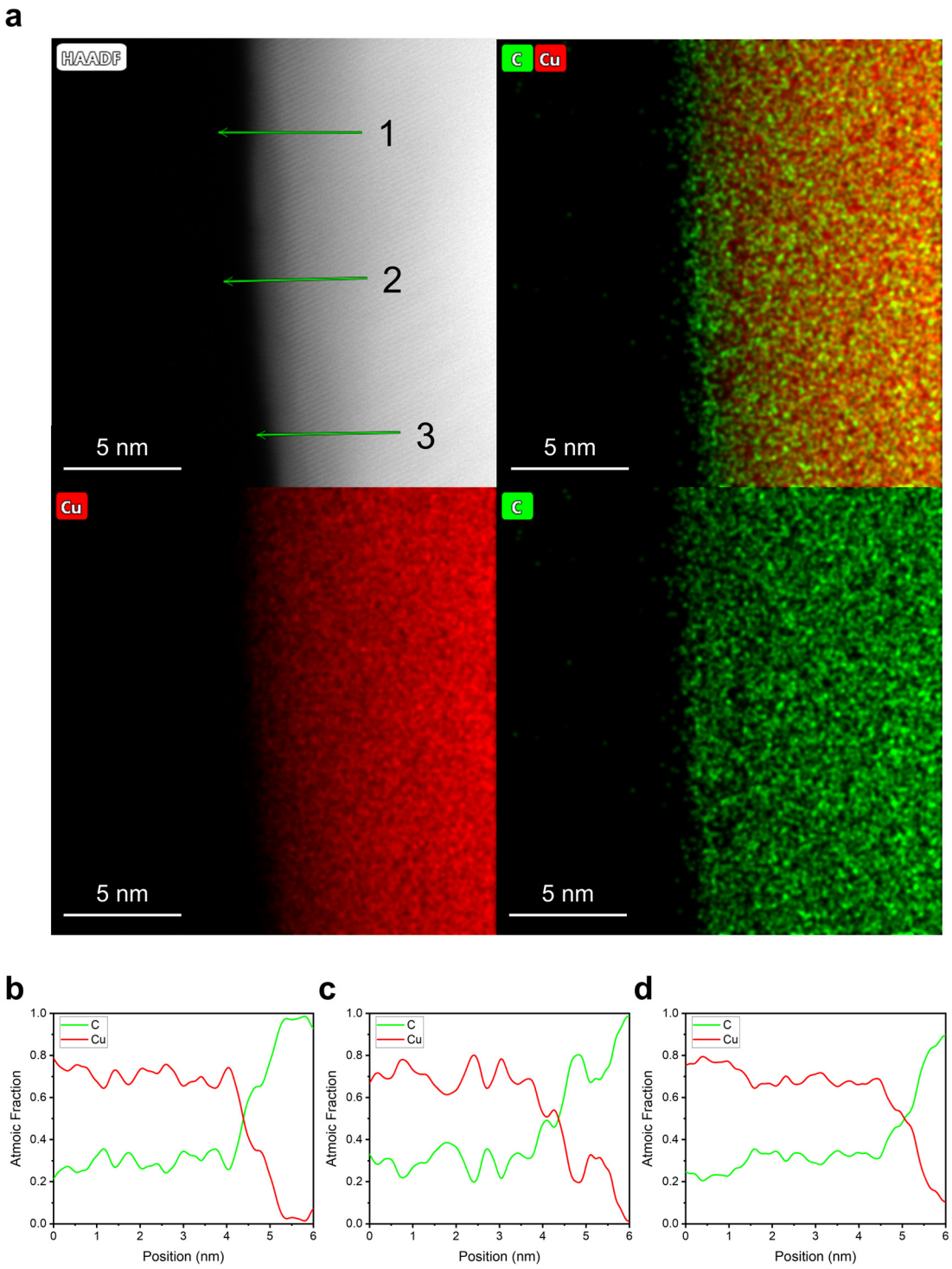

Fig. S10 (a) HRTEM-HAADF-EDS images of C shell-covered Cu nanoparticle in Cu/CNFs (40%)_SO. These images reveal C shell formation on Cu by Boudouard reaction. Line profiles of HRTEM-HAADF-EDS image about C shell-covered Cu nanoparticle in Cu/CNFs (40%)_SO at (b) number 1 location, (c) number 2 location, and (d) number 3 location. The direction of the lines was from core of Cu to surface of Cu.

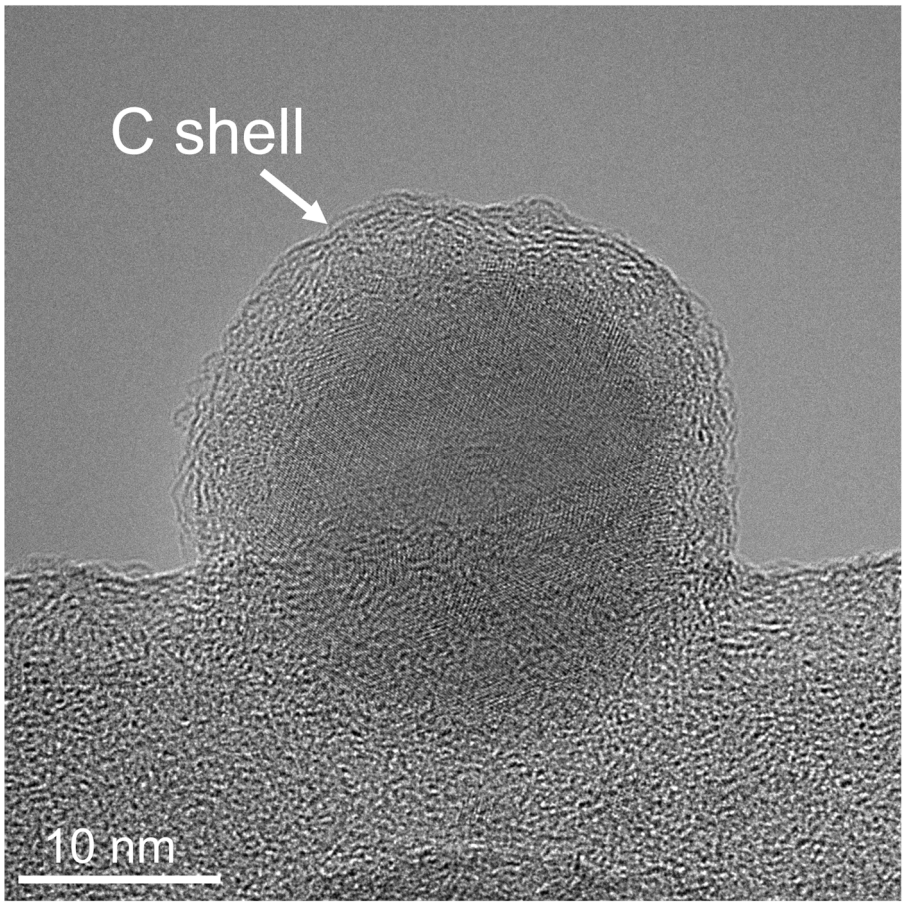

Fig. S11 HRTEM image of C shell-covered Cu nanoparticle in Cu/CNFs (60%)_SO. The thickness of C shell is about 4 nm.

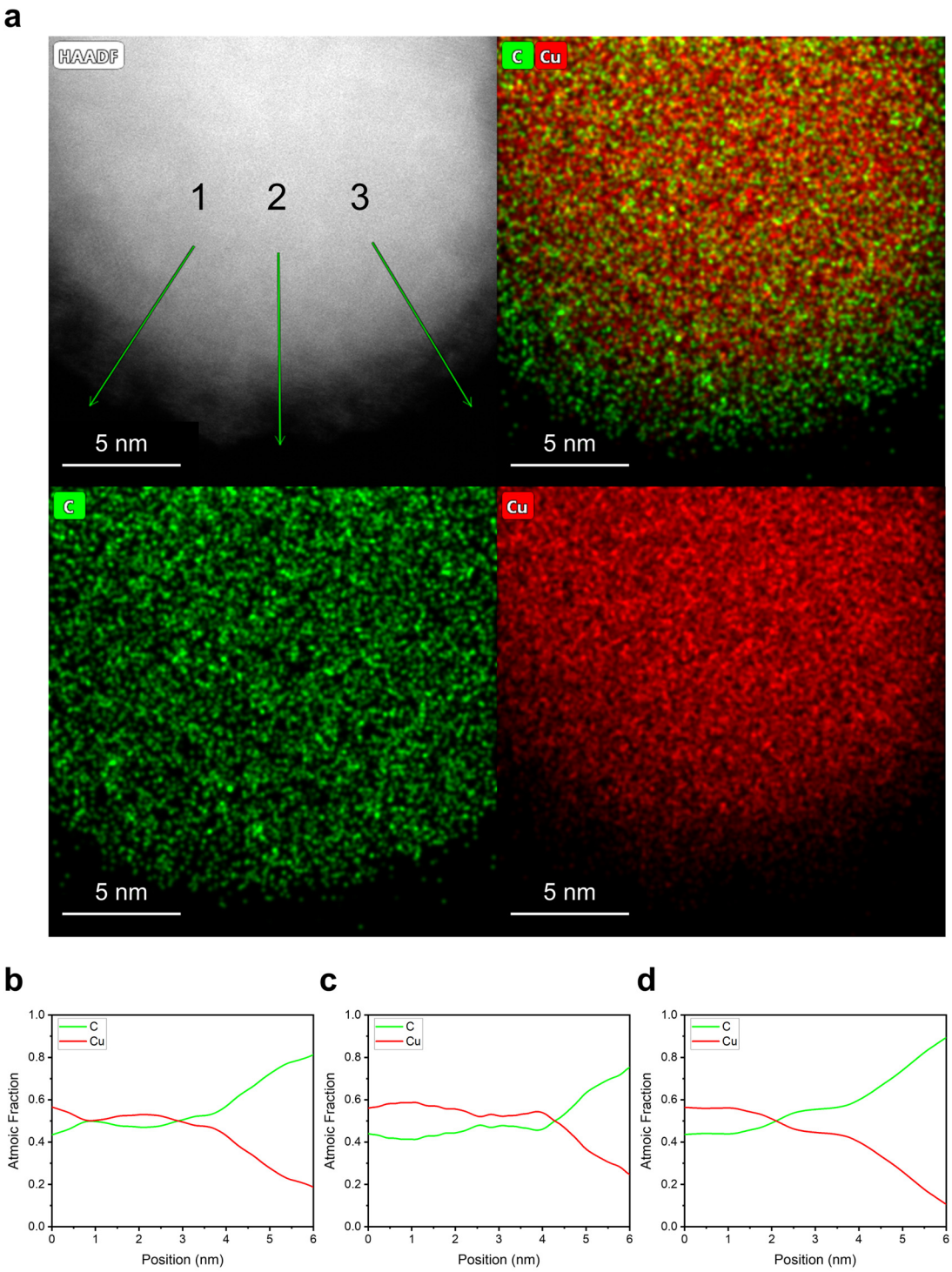

Fig. S12 (a) HRTEM-HAADF-EDS images of C shell-covered Cu nanoparticle in Cu/CNFs (60%)_SO. Line profiles of HRTEM-HAADF-EDS image about C shell-covered Cu nanoparticle in Cu/CNFs (60%)_SO at (b) number 1 location, (c) number 2 location, and (d) number 3 location. The direction of the lines was from core of Cu to surface of Cu.

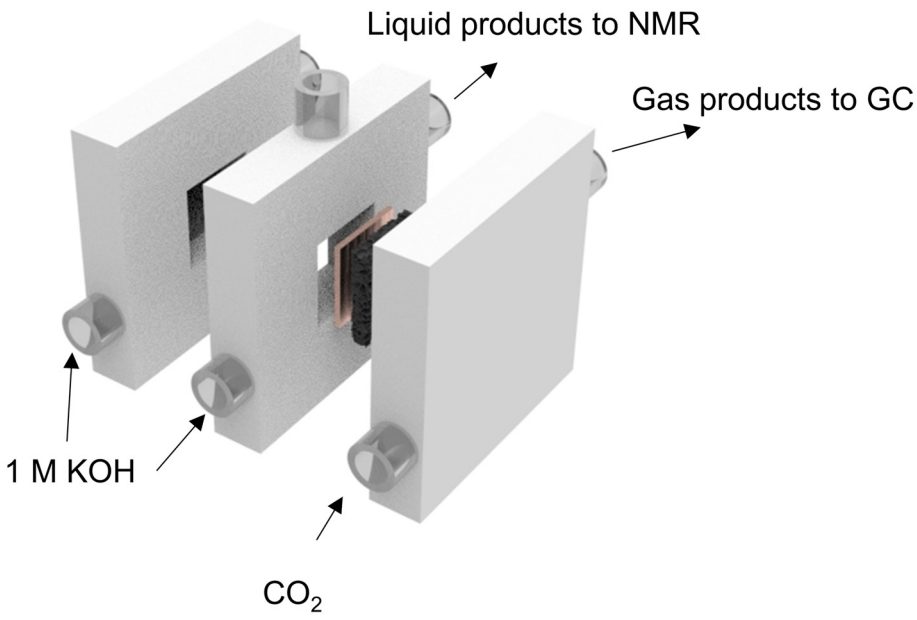

Fig. S13 Schematic of the home-made flow cell with three parts.

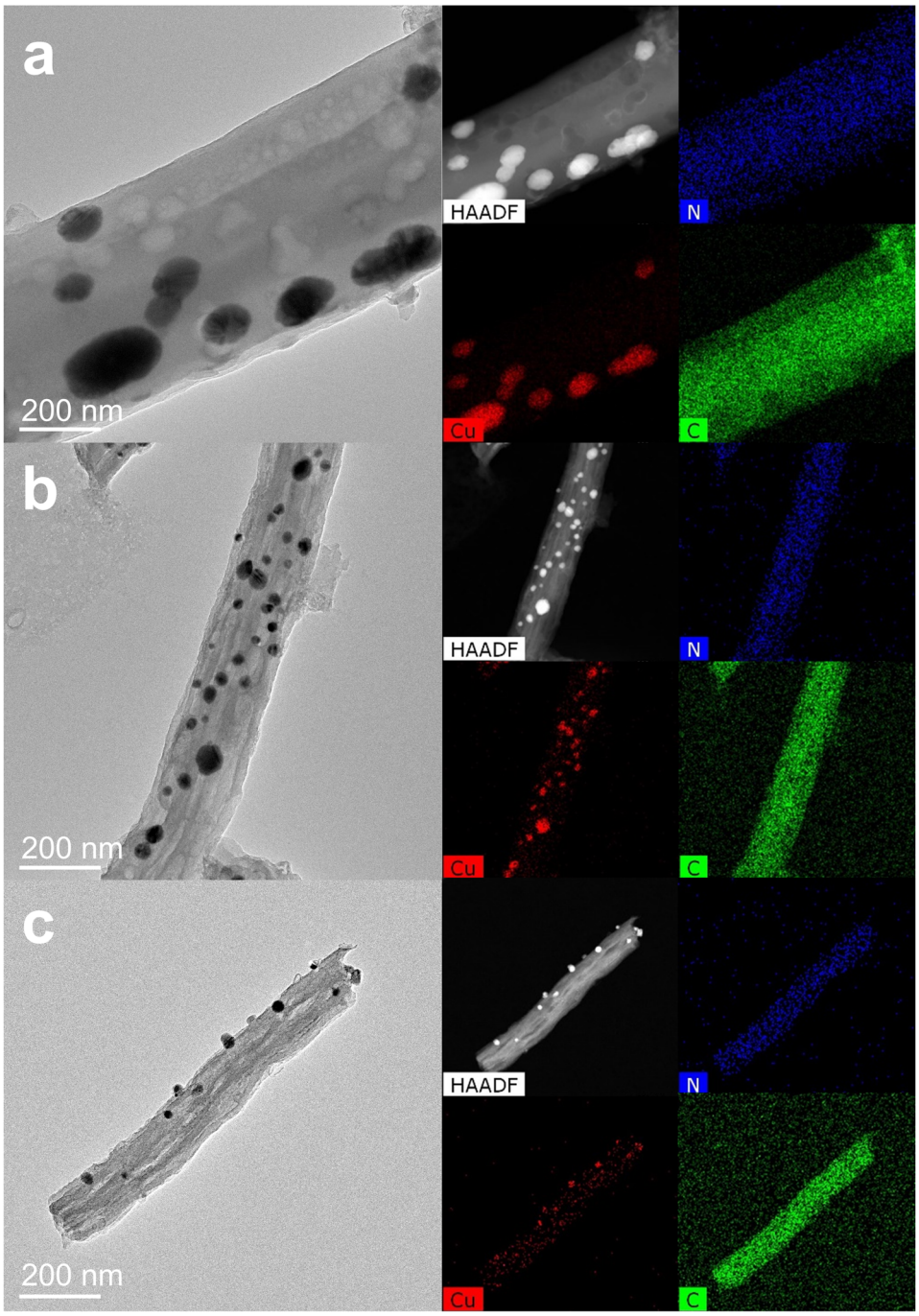

Fig. S14 TEM-EDS images of Cu/CNFs (*X*%)_FR after CO_2RR. (a) Cu/CNFs (0%)_FR, (b) Cu/CNFs (40%)_FR, and (c) Cu/CNFs (60%)_FR.

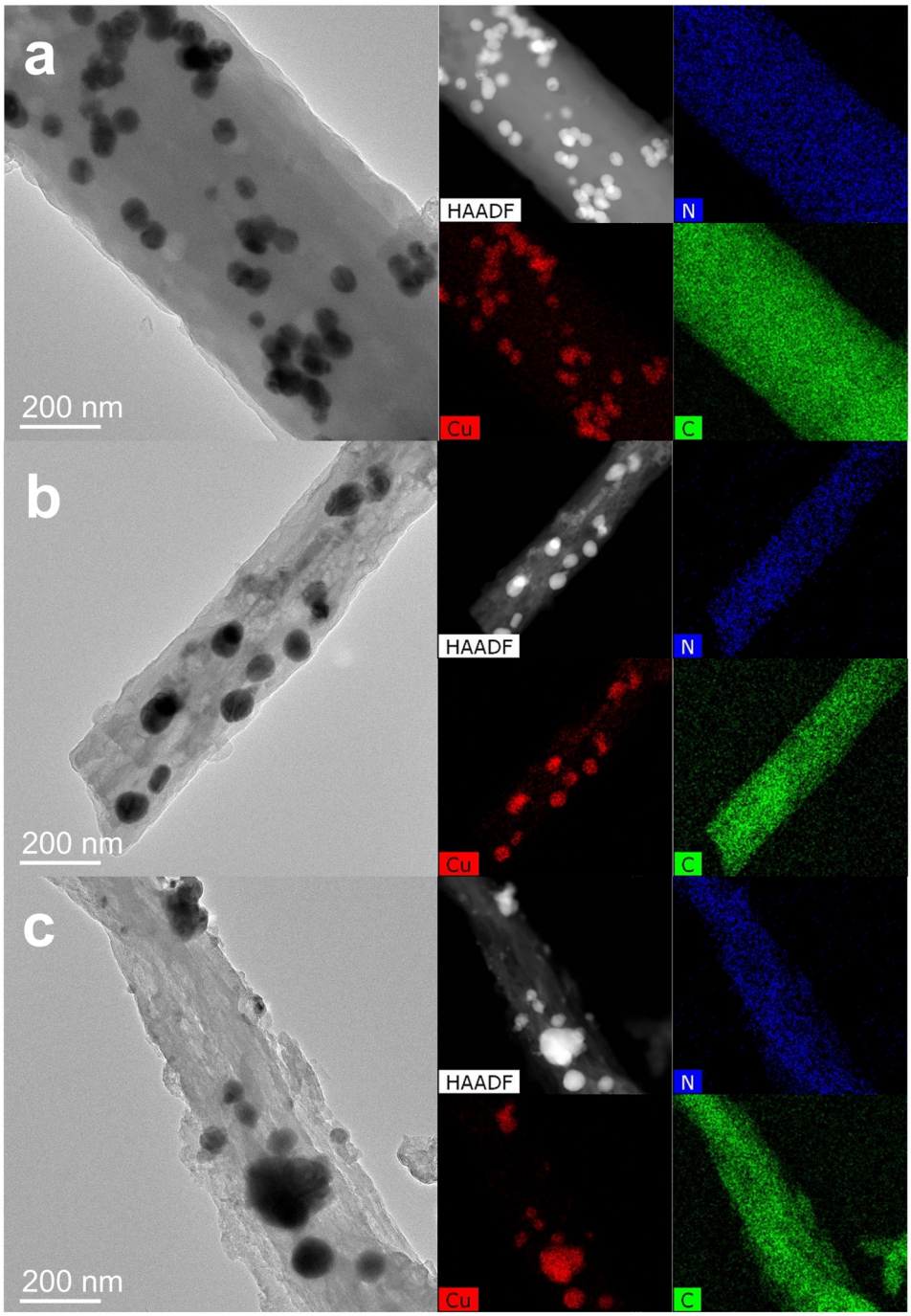

Fig. S15 TEM-EDS images of Cu/CNFs (*X*%)_SO after CO_2RR. (a) Cu/CNFs (0%)_SO, (b) Cu/CNFs (40%)_SO, and (c) Cu/CNFs (60%)_SO.

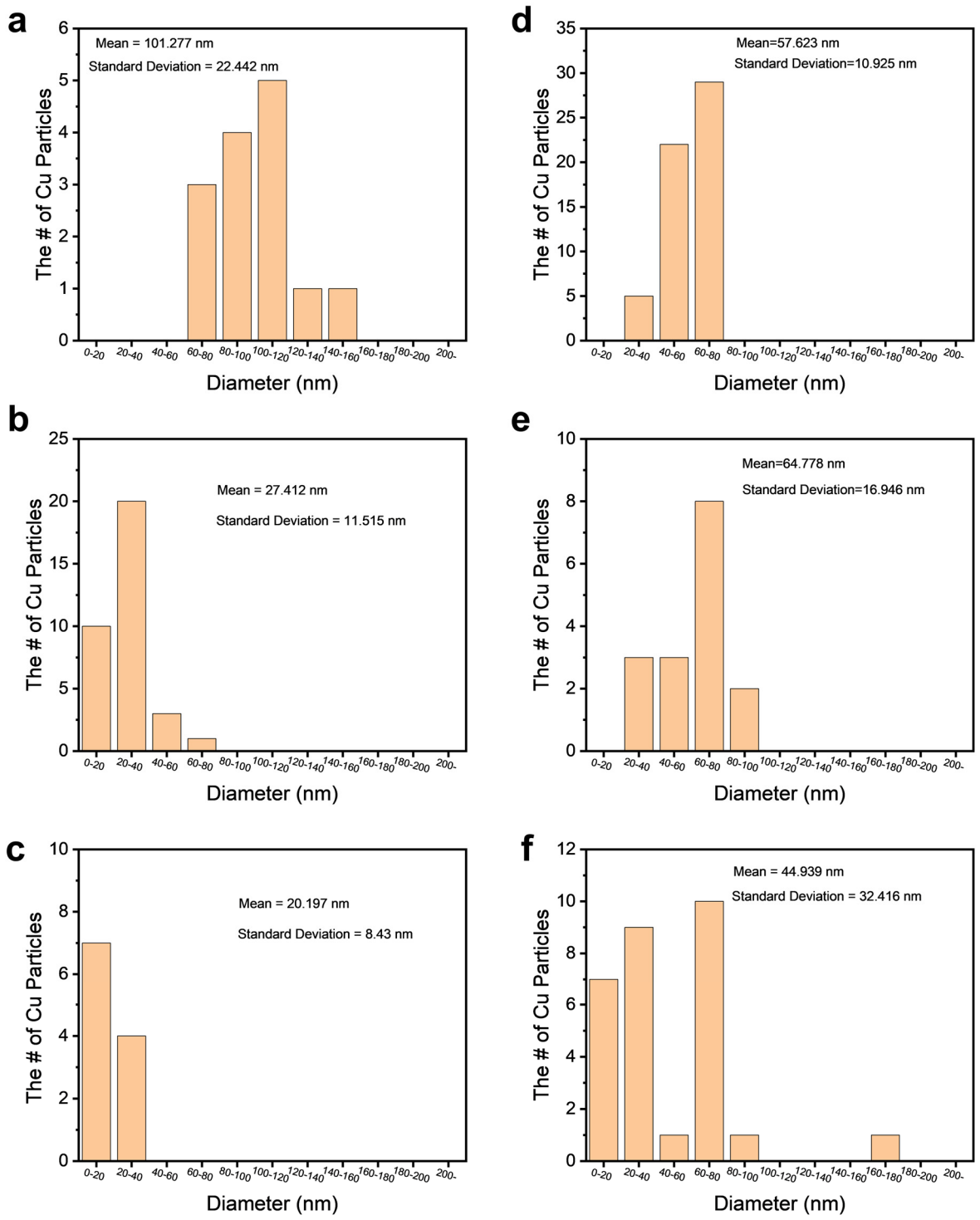

Fig. S16 Cu particle sizes distributions in Cu/CNFs after CO_2RR represented by histograms. (a) Cu/CNFs (0%)_FR, (b) Cu/CNFs (40%)_FR, (c) Cu/CNFs (60%)_FR, (d) Cu/CNFs (0%)_SO, (e) Cu/CNFs (40%)_SO, and (f) Cu/CNFs (60%)_SO. Cu particle sizes were analyzed based on TEM images.

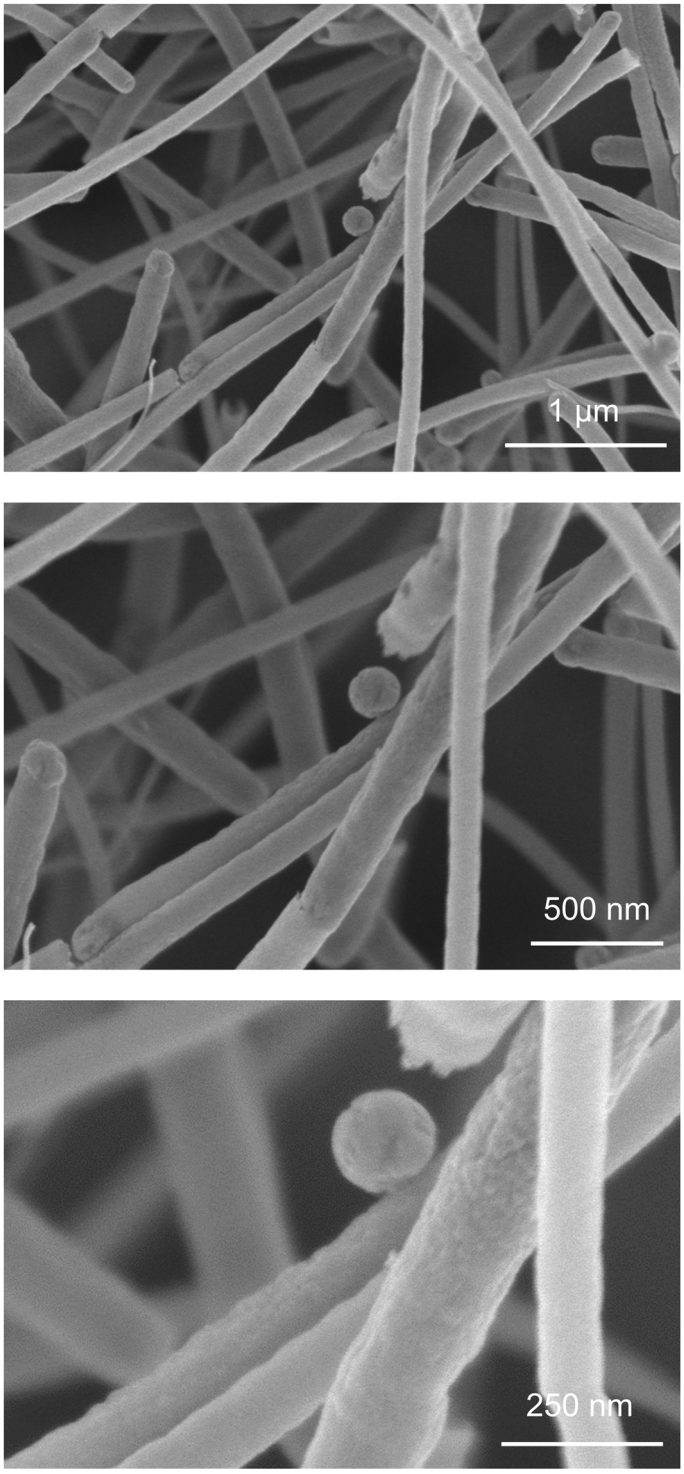

Fig. S17 SEM images of diameter-controlled Cu/CNFs (0%)_SO with various magnifications. The diameter is about 165 nm.

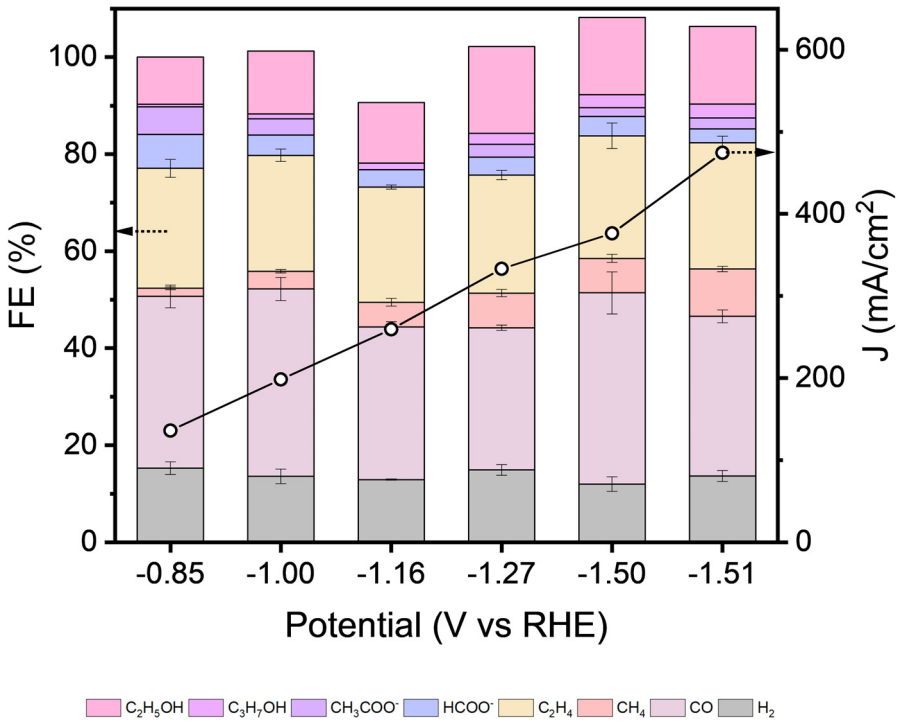

Fig. S18 CO_2RR performances of diameter-controlled Cu/CNFs (0%)_SO. The performances are disparate with those of Cu/CNFs (60%)_SO.

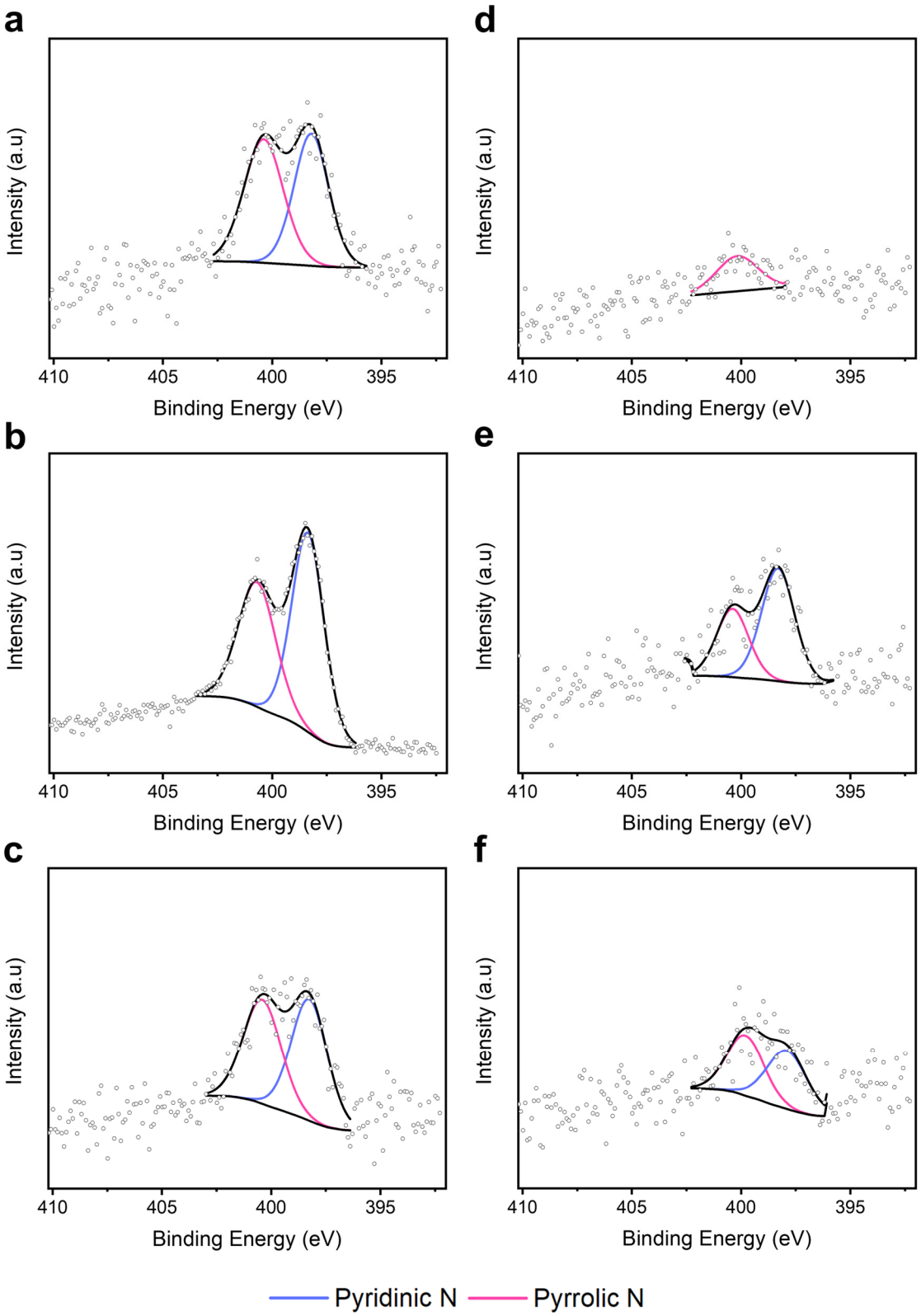

Fig. S19 N 1s XPS spectra of Cu/CNFs. Pyridinic N (~398.2 eV) and pyrrolic N (~400.1 eV) of (a) Cu/CNFs (0%)_FR, (b) Cu/CNFs (40%)_FR, (c) Cu/CNFs (60%)_FR, (d) Cu/CNFs (0%)_SO, (e) Cu/CNFs (40%)_SO, and (f) Cu/CNFs (60%)_SO.[3]

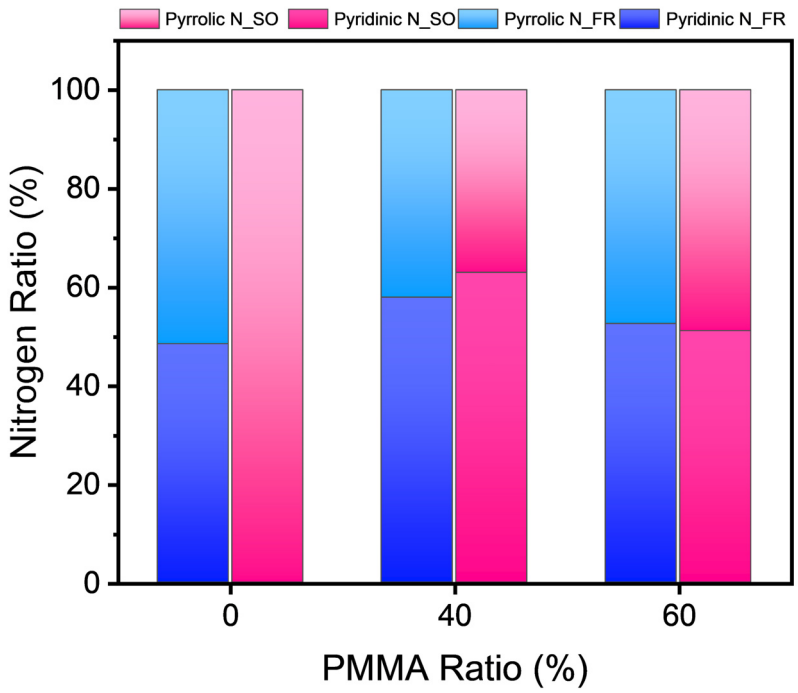

Fig. S20 The integral area ratio of pyridinic N and pyrrolic N based on PMMA ratio and calcination conditions analyzed by XPS about N 1s.

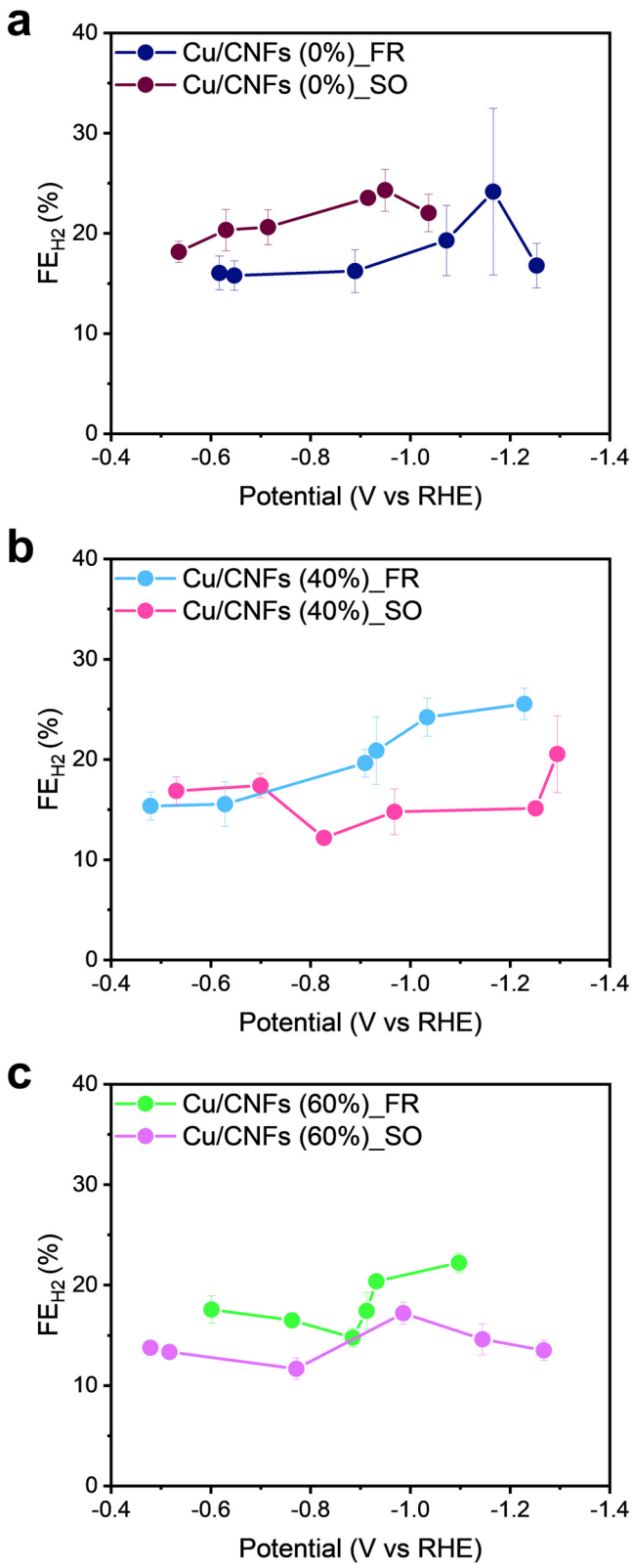

Fig. S21 H_2 FE comparison between (a) Cu/CNFs (0%)_FR and Cu/CNFs (0%)_SO, (b) Cu/CNFs (40%)_FR and Cu/CNFs (40%)_SO, and (c) Cu/CNFs (60%)_FR and Cu/CNFs (60%)_SO.

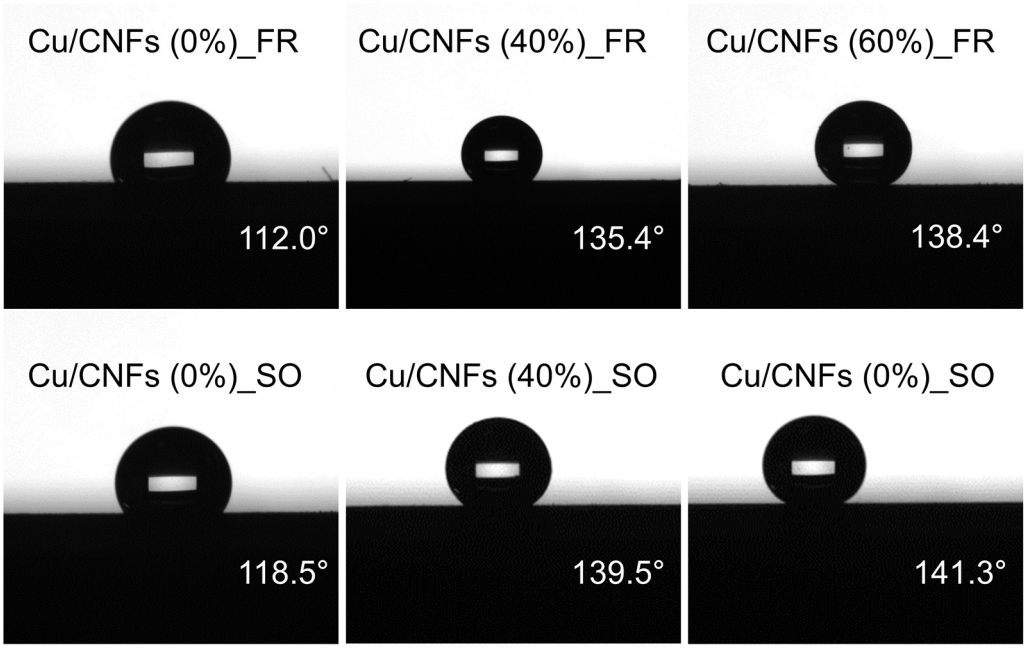

Fig. S22 Contact angle images of Cu/CNFs. The samples were fabricated by spraying catalyst ink on silicon wafers as a substrate.

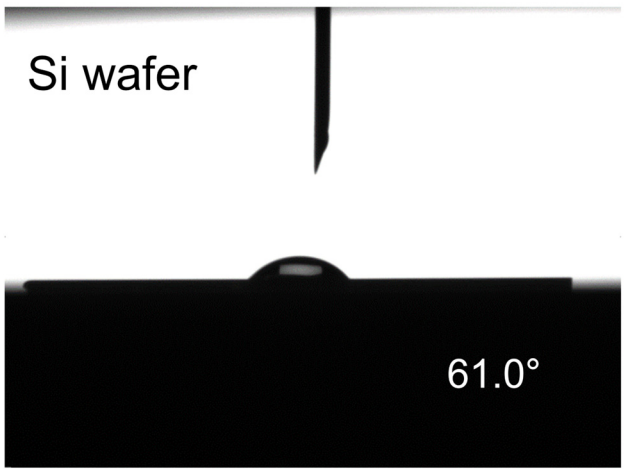

Fig. S23 A contact angle image of a silicon wafer as the substrate for contact angle measurements.

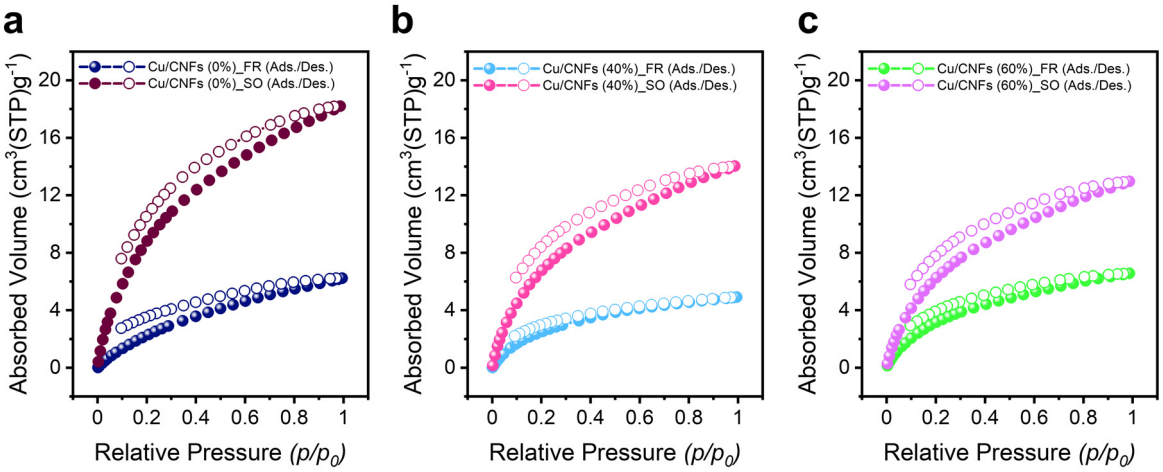

Fig. S24 CO_2 adsorption and desorption of Cu/CNFs according to the relative pressures from 0 to 0.99. (a) Cu/CNFs (0%)_FR and Cu/CNFs (0%)_SO, (b) Cu/CNFs (40%)_FR and Cu/CNFs (40%)_SO, and (c) Cu/CNFs (60%)_FR and Cu/CNFs (60%)_SO.

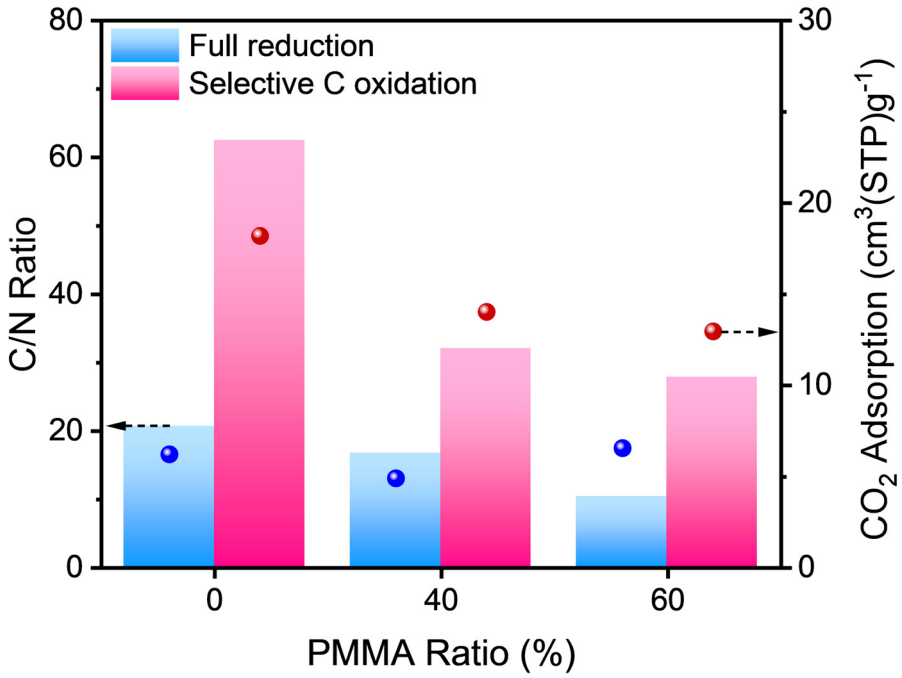

Fig. S25 The correlation between surface C/N ratio and CO_2 adsorption ability of Cu/CNFs. CO_2 adsorption at 0.99 relative pressure followed surface C/N ratio.

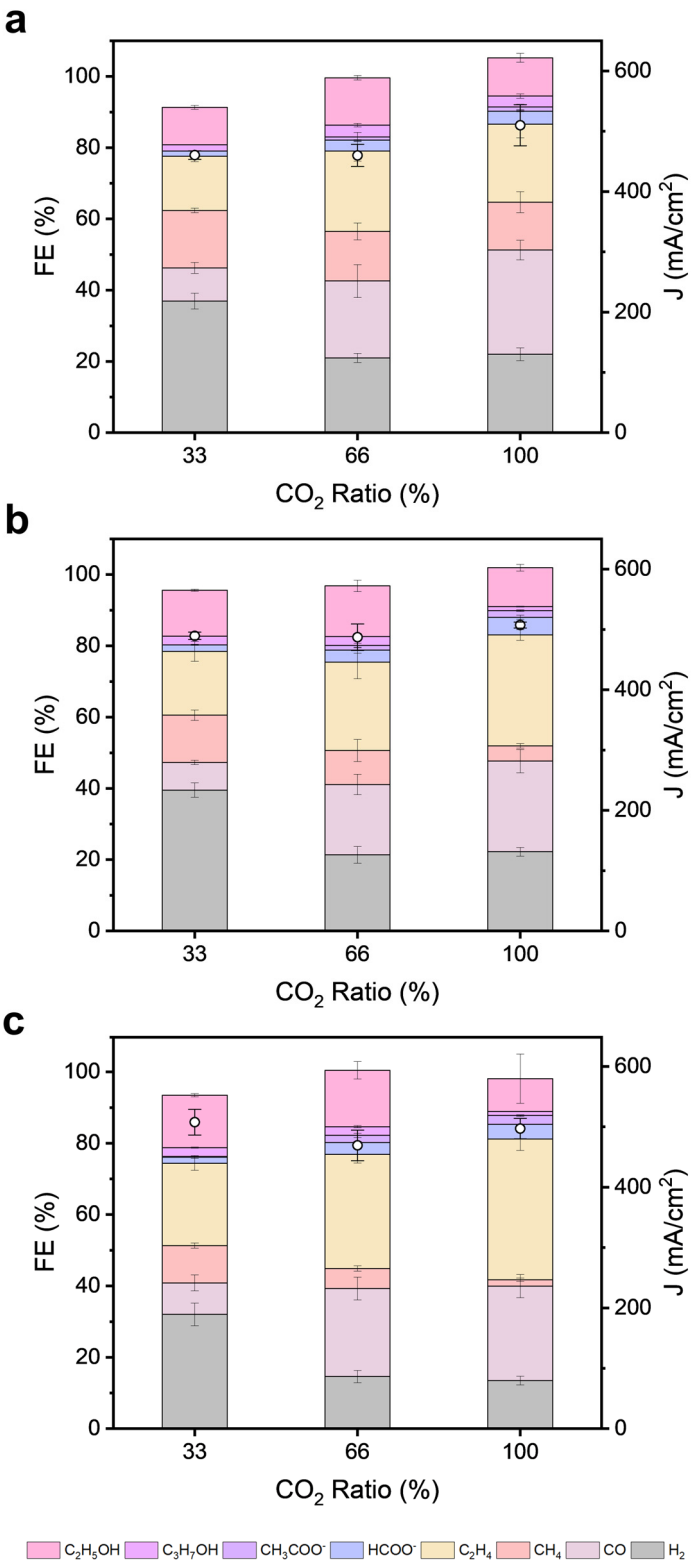

Fig. S26 CO_2RR performances at -3.4 V (vs RHE, non-iR corrected) by varying the CO_2 ratio in CO_2 + Ar mixed gas. (a) Cu/CNFs (0%)_SO, (b) Cu/CNFs (60%)_FR, and (c) Cu/CNFs (60%)_SO.

Table S1. Pore size distribution of Cu/CNFs with surface areas and pore volumes acquired by BJH plot.

	Cu/CNFs (0%)_FR	Cu/CNFs (40%)_FR	Cu/CNFs (60%)_FR	Cu/CNFs (0%)_SO	Cu/CNFs (40%)_SO	Cu/CNFs (60%)_SO
Total surface area (m^2/g)	7.484	27.244	44.282	8.149	41.684	42.035
Micropores	0.734	0.249	2.262	0.582	0.554	0.000
Mesopores	5.920	24.750	38.353	6.711	38.438	39.576
Macropores	0.830	2.245	3.667	0.856	2.692	2.459
Total pore volume (cm^3/g)	0.0324	0.1263	0.2099	0.0341	0.1877	0.2102
Micropores	0.0000	0.0000	0.0021	0.0000	0.0012	0.0000
Mesopores	0.0144	0.0708	0.1305	0.0155	0.1298	0.1404
Macropores	0.0180	0.0555	0.0773	0.0186	0.0567	0.0698

Table S2. Intensity of D band over intensity of G band ratio of Cu/CNFs obtained by Raman spectroscopy.

Calcination process	0% of PMMA ratio	40% of PMMA ratio	60% of PMMA ratio
Full reduction	1.02	1.02	1.01
Selective C oxidation	1.02	0.96	0.95

Table. S3 Average FEs and standard deviations of each CO_2RR product about Cu/CNFs (0%)_FR. The values were calculated by data from three samples for each potential.

Products	Value (%)	-0.62 V (vs RHE)	-0.65 V (vs RHE)	-0.89 V (vs RHE)	-1.07 V (vs RHE)	-1.17 V (vs RHE)	-1.25 V (vs RHE)
H_2	Average FE	16.2	15.8	16.4	18.8	24.2	16.8
	Standard deviation	1.8	1.9	2.8	3.7	8.1	2.5
CO	Average FE	52.7	52.1	47.2	42.3	37.2	30.7
	Standard deviation	9.0	4.9	9.5	6.2	10.3	10.8
CH_4	Average FE	1.4	1.8	2.6	5.6	6.2	4.1
	Standard deviation	0.7	0.6	0.7	4.1	3.8	1.5
C_2H_4	Average FE	14.5	15.8	16.6	21.5	20.7	23.2
	Standard deviation	4.1	4.2	4.0	3.4	5.0	3.8
$HCOO^-$	Average FE	9.8	8.3	7.5	6.1	7.9	5.5
	Standard deviation	1.3	1.5	2.4	0.3	4.1	2.0
C_3H_7OH	Average FE	0.9	1.6	1.4	1.4	2.1	2.0
	Standard deviation	0.8	0.7	1.0	2.4	0.4	0.6
CH_3COO^-	Average FE	0.5	0.7	2.3	1.5	2.0	2.3
	Standard deviation	0.5	0.3	2.7	0.3	1.0	0.7
C_2H_5OH	Average FE	5.2	5.6	4.0	7.5	6.4	9.4
	Standard deviation	0.5	1.9	1.7	1.5	3.8	2.7

Table. S4 Average FEs and standard deviations of each CO_2RR product about Cu/CNFs (40%)_FR. The values were calculated by data from three samples for each potential.

Products	Value (%)	-0.48 V (vs RHE)	-0.63 V (vs RHE)	-0.91 V (vs RHE)	-0.93 V (vs RHE)	-1.03 V (vs RHE)	-1.23 V (vs RHE)
H_2	Average FE	15.4	15.2	19.6	21.2	24.2	25.5
	Standard deviation	1.5	2.4	2.2	3.2	2.0	1.9
CO	Average FE	33.7	41.7	44.1	32.3	33.7	34.8
	Standard deviation	4.5	7.3	4.9	4.4	4.4	2.1
CH_4	Average FE	0.4	0.5	0.6	1.4	2.1	2.8
	Standard deviation	0.3	0.2	0.3	0.4	0.8	0.4
C_2H_4	Average FE	23.6	19.9	18.1	21.6	23.9	23.6
	Standard deviation	2.0	4.6	3.5	3.4	1.6	0.6
$HCOO^-$	Average FE	14.3	16.0	15.8	12.2	9.0	6.4
	Standard deviation	1.4	2.1	2.7	2.8	3.3	0.3
C_3H_7OH	Average FE	3.8	3.6	1.4	3.2	3.4	2.0
	Standard deviation	0.4	1.5	1.0	0.2	1.1	0.4
CH_3COO^-	Average FE	1.8	0.5	0.3	0.5	0.6	0.8
	Standard deviation	2.0	0.3	0.1	0.2	0.1	0.1
C_2H_5OH	Average FE	7.6	6.9	5.3	7.0	8.2	8.4
	Standard deviation	1.0	3.5	0.2	1.7	1.6	0.2

Table. S5 Average FEs and standard deviations of each CO_2RR product about Cu/CNFs (60%)_FR. The values were calculated by data from three samples for each potential.

Products	Value (%)	-0.60 V (vs RHE)	-0.76 V (vs RHE)	-0.88 V (vs RHE)	-0.91 V (vs RHE)	-0.93 V (vs RHE)	-1.10 V (vs RHE)
H_2	Average FE	17.6	16.5	14.8	17.3	20.4	22.2
	Standard deviation	1.3	1.7	1.5	1.9	0.7	1.2
CO	Average FE	42.9	35.9	29.5	24.6	27.9	25.4
	Standard deviation	3.6	4.8	3.4	1.8	3.6	3.3
CH_4	Average FE	0.6	1.4	2.1	4.2	3.4	4.3
	Standard deviation	0.4	0.4	0.4	0.7	0.4	0.6
C_2H_4	Average FE	21.3	24.2	33.1	34.4	32.1	31.1
	Standard deviation	3.6	4.0	2.8	1.5	0.7	1.5
$HCOO^-$	Average FE	15.8	14.0	6.8	4.4	4.6	5.0
	Standard deviation	1.3	2.9	0.5	0.5	0.3	0.6
C_3H_7OH	Average FE	2.4	2.9	2.7	2.1	1.6	1.9
	Standard deviation	1.2	0.8	0.6	0.4	0.3	0.3
CH_3COO^-	Average FE	0.5	0.5	1.1	1.3	1.3	1.1
	Standard deviation	0.1	0.2	0.1	0.2	0.1	0.1
C_2H_5OH	Average FE	6.6	7.4	11.0	11.9	11.4	10.9
	Standard deviation	1.4	1.1	0.8	0.8	1.1	0.9

Table. S6 Average FEs and standard deviations of each CO_2RR product about Cu/CNFs (0%)_SO. The values were calculated by data from three samples for each potential.

Products	Value (%)	-0.54 V (vs RHE)	-0.63 V (vs RHE)	-0.71 V (vs RHE)	-0.91 V (vs RHE)	-0.95 V (vs RHE)	-1.04 V (vs RHE)
H_2	Average FE	18.2	20.3	20.6	23.5	24.3	22.0
	Standard deviation	1.2	2.0	1.6	2.1	2.4	1.8
CO	Average FE	41.9	39.9	35.8	27.4	27.4	29.2
	Standard deviation	3.8	2.8	2.2	1.6	6.4	2.8
CH_4	Average FE	4.7	4.7	5.5	15.0	12.7	13.4
	Standard deviation	1.4	0.7	0.4	1.5	5.2	2.9
C_2H_4	Average FE	20.9	21.3	19.5	19.8	21.5	21.9
	Standard deviation	3.6	1.7	2.4	2.2	3.7	3.8
$HCOO^-$	Average FE	6.9	5.9	5.5	4.4	3.7	3.6
	Standard deviation	1.7	0.5	0.4	0.3	0.6	0.1
C_3H_7OH	Average FE	1.6	2.2	1.3	2.0	1.2	1.2
	Standard deviation	1.2	0.6	0.2	0.3	0.4	0.7
CH_3COO^-	Average FE	1.6	1.3	1.5	3.2	2.9	3.0
	Standard deviation	0.5	0.2	0.0	0.2	0.6	0.6
C_2H_5OH	Average FE	8.1	9.7	11.6	11.0	12.0	10.8
	Standard deviation	0.9	1.1	1.6	0.7	0.4	1.3

Table. S7 Average FEs and standard deviations of each CO_2RR product about Cu/CNFs (40%)_SO. The values were calculated by data from three samples for each potential.

Products	Value (%)	-0.53 V (vs RHE)	-0.70 V (vs RHE)	-0.83 V (vs RHE)	-0.97 V (vs RHE)	-1.25 V (vs RHE)	-1.29 V (vs RHE)
H_2	Average FE	16.9	17.4	12.2	14.8	15.1	20.5
	Standard deviation	2.2	1.6	0.5	2.1	0.9	3.4
CO	Average FE	42.0	29.6	30.8	28.7	29.1	27.6
	Standard deviation	6.4	4.8	4.4	3.8	2.3	2.3
CH_4	Average FE	1.1	2.4	0.6	2.3	3.4	6.0
	Standard deviation	0.2	1.1	0.2	1.1	0.8	1.6
C_2H_4	Average FE	16.2	27.9	33.2	31.6	29.0	28.0
	Standard deviation	4.7	2.7	3.8	3.4	1.9	1.5
$HCOO^-$	Average FE	12.7	8.7	8.2	6.9	4.9	3.9
	Standard deviation	0.7	0.6	1.5	0.7	0.7	0.4
C_3H_7OH	Average FE	3.8	3.1	4.5	3.3	2.9	2.0
	Standard deviation	0.7	0.6	0.1	0.9	0.4	0.6
CH_3COO^-	Average FE	0.7	1.1	0.8	1.5	1.8	2.0
	Standard deviation	0.0	0.4	0.1	0.5	0.4	0.5
C_2H_5OH	Average FE	6.7	10.1	12.1	14.4	13.7	12.7
	Standard deviation	1.5	1.1	1.1	2.1	0.6	0.8

Table. S8 Average FEs and standard deviations of each CO_2RR product about Cu/CNFs (60%)_SO. The values were calculated by data from three samples for each potential.

Products	Value (%)	-0.48 V (vs RHE)	-0.52 V (vs RHE)	-0.77 V (vs RHE)	-0.99 V (vs RHE)	-1.14 V (vs RHE)	-1.27 V (vs RHE)
H_2	Average FE	13.8	13.3	11.7	17.2	14.6	13.5
	Standard deviation	1.5	1.0	1.4	1.7	1.8	1.2
CO	Average FE	34.4	29.8	31.9	33.9	29.0	26.4
	Standard deviation	4.3	2.3	3.7	3.6	4.6	3.2
CH_4	Average FE	0.6	1.0	0.9	2.3	1.8	1.8
	Standard deviation	0.4	0.1	0.5	0.5	0.4	0.5
C_2H_4	Average FE	30.2	36.7	35.7	31.9	35.8	39.5
	Standard deviation	4.2	3.4	3.9	1.3	4.2	3.2
$HCOO^-$	Average FE	9.9	7.0	6.4	5.0	4.6	4.1
	Standard deviation	1.4	0.7	1.2	0.2	0.1	0.1
C_3H_7OH	Average FE	3.3	3.5	3.7	2.7	2.5	2.5
	Standard deviation	0.3	0.3	0.7	0.6	0.1	0.2
CH_3COO^-	Average FE	0.8	0.8	0.7	1.0	0.9	1.1
	Standard deviation	0.1	0.2	0.1	0.2	0.1	0.0
C_2H_5OH	Average FE	8.7	10.8	11.7	9.3	11.5	9.2
	Standard deviation	1.7	1.4	1.3	0.5	1.5	6.9

Table. S9 Average FEs and standard deviations of each CO_2RR product at -3.4 V (vs RHE, non-iR corrected) under 33% and 66% of CO_2 ratio in CO_2+Ar mixed gas about Cu/CNFs (0%)_SO, Cu/CNFs (60%)_FR and Cu/CNFs (60%)_SO. The values were calculated by data from three samples for each potential.

Products	Value (%)	Cu/CNFs (0%)_SO		Cu/CNFs (60%)_FR		Cu/CNFs (60%)_SO	
		33% of CO_2 ratio	66% of CO_2 ratio	33% of CO_2 ratio	66% of CO_2 ratio	33% of CO_2 ratio	66% of CO_2 ratio
H_2	Average FE	37.0	21.0	39.5	21.4	32.0	14.6
	Standard deviation	2.2	1.3	2.0	2.3	3.2	1.7
CO	Average FE	9.3	21.6	7.7	19.7	8.8	24.7
	Standard deviation	1.5	4.6	0.6	2.9	2.2	3.2
CH_4	Average FE	16.2	13.9	13.3	9.5	10.5	5.6
	Standard deviation	0.6	2.4	1.5	3.1	0.7	0.7
C_2H_4	Average FE	15.2	22.6	17.9	24.8	23.1	32.0
	Standard deviation	1.5	2.8	2.8	4.7	2.0	2.4
$HCOO^-$	Average FE	1.4	3.1	1.8	3.3	1.7	3.3
	Standard deviation	0.1	0.1	0.1	0.8	0.3	0.4
C_3H_7OH	Average FE	0.0	0.9	0.0	1.3	0.2	2.0
	Standard deviation	0.0	1.3	0.0	0.6	0.2	0.6
CH_3COO^-	Average FE	1.8	3.3	2.4	2.5	2.5	2.4
	Standard deviation	0.0	0.5	0.1	0.3	0.1	0.3
C_2H_5OH	Average FE	10.5	13.3	12.9	14.2	14.7	15.8
	Standard deviation	0.5	0.6	0.3	1.6	0.4	2.4

Table S10. Ratio of $CO_{atop,\ HFB}/(CO_{atop,\ HFB}+CO_{atop,\ LFB})$ about Cu/CNFs (*X*%)_SO with different porosity analyzed by *in-situ* Raman spectroscopy.

Applied potential	Cu/CNFs (0%)_SO	Cu/CNFs (40%)_SO	Cu/CNFs (60%)_SO
-0.1 V (vs RHE)	0.471	0.569	0.578
-0.2 V (vs RHE)	0.404	0.554	0.645
-0.3 V (vs RHE)	0.362	0.626	0.627

References

1. H. Jung, S. Y. Lee, C. W. Lee, M. K. Cho, D. H. Won, C. Kim, H. S. Oh, B. K. Min and Y. J. Hwang, *J. Am. Chem. Soc.*, 2019, **141**, 4624-4633.
2. R. Hassanien, M. M. Almaky, A. Houlton and B. R. Horrocks, *RSC Adv.*, 2016, **6**, 99422-99432.
3. J. Wu, R. M. Yadav, M. Liu, P. P. Sharma, C. S. Tiwary, L. Ma, X. Zou, X.-D. Zhou, B. I. Yakobson, J. Lou and P. M. Ajayan, *ACS Nano*, 2015, **9**, 5364-5371.